2011 50th IEEE Conference on Decision and Control and
European Control Conference (CDC-ECC)
Orlando, FL, USA, December 12-15, 2011

A Near-Real Time Nonlinear State Estimation Approach with Application to Initialization of Navigation Systems

Arvind Ramanandan
arama004@ucr.edu

Anning Chen
achen028@ucr.edu

Jay A. Farrell
farrell@ee.ucr.edu

***Abstract*—The performance of any linearization based estimation algorithm like the Extended Kalman Filter (EKF) relies heavily on the accuracy of the nominal trajectory about which the system is linearized. When the linearization assumption does not hold, such an algorithm behaves in an unpredictable fashion and metrics of estimation error (i.e. state covariance) are invalid.**

This paper presents methods to identify in real-time those parts of the state vector whose uncertainties cause significant deviations from the linearized model and proposes a near-real time approach to address the issue. One important class of applications is initialization of navigation systems; therefore, as an example the paper applies the results of the theory to a simplified 7 state, two dimensional GPS aided INS. The near-real time approach is demonstrated in simulation.

I. Introduction

Consider evolution of state $\boldsymbol{x}$ in the state space $\mathbb{R}^N$ according to some nonlinear vector of real analytic mappings $\boldsymbol{f} : \mathbb{R}^{N+M} \rightarrow \mathbb{R}^N$ defined by

$$\dot{\boldsymbol{x}} = \boldsymbol{f}(\boldsymbol{x}, \boldsymbol{u}) \tag{1}$$

where $\boldsymbol{u} \in \mathbb{R}^M$ denotes the inputs to the system. If the system dynamics $\boldsymbol{f}$ and initial conditions are perfectly known, the state $\boldsymbol{x}$ can be uniquely determined by integrating (1). But in real-world scenarios, $\boldsymbol{u} \in \mathbb{R}^M$ are unknown and we are only equipped with non-ideal sensors that make noisy measurements of $\boldsymbol{u}$ denoted by $\tilde{\boldsymbol{u}}$. Also, the initial conditions $\boldsymbol{x}(0)$ are not perfectly known at time $t = 0$. Hence an estimate of the state, $\hat{\boldsymbol{x}}$, is computed by integrating $\dot{\hat{\boldsymbol{x}}} = \boldsymbol{f}(\hat{\boldsymbol{x}}, \tilde{\boldsymbol{u}})$. But note that $\hat{\boldsymbol{x}}$ is a stochastic process as the inputs $\tilde{\boldsymbol{u}}$ and initial conditions $\boldsymbol{x}(0)$ are random in nature.

Assume that we are equipped with sensors that measure some function of the state $\boldsymbol{x}$ modeled as

$$\tilde{\boldsymbol{y}} = \boldsymbol{h}(\boldsymbol{x}) + \boldsymbol{n} \tag{2}$$

where $\boldsymbol{h} : \mathbb{R}^N \rightarrow \mathbb{R}^P$ is a vector of real analytic functions and $\boldsymbol{n} \in \mathbb{R}^P$ is additive noise. Under the Bayesian estimation philosophy (Ch. 10 in [8]), an estimator of $\boldsymbol{x}$ may be defined as

$$\hat{\boldsymbol{x}} = \arg\max_{\boldsymbol{x} \in \mathbb{R}^N} \left(p\{\boldsymbol{x}|\tilde{\boldsymbol{y}}, \tilde{\boldsymbol{u}}\}\right) = \arg\max_{\boldsymbol{x} \in \mathbb{R}^N} \left(p\{\tilde{\boldsymbol{y}}|\boldsymbol{x}, \tilde{\boldsymbol{u}}\} p\{\boldsymbol{x}, \tilde{\boldsymbol{u}}\}\right) \tag{3}$$

where $p\{\boldsymbol{x}|\tilde{\boldsymbol{y}}, \tilde{\boldsymbol{u}}\}\}$ denotes the probability density of state $\boldsymbol{x}$ conditioned on the measurements $\tilde{\boldsymbol{y}}$ and inputs $\tilde{\boldsymbol{u}}$. Computation of the joint probability $p\{\tilde{\boldsymbol{y}}|\boldsymbol{x}, \tilde{\boldsymbol{u}}\}$ is tractable as the random noise appears additively in the model depicted in (2), however computing the stochastic properties of $\boldsymbol{x}$, characterized by the joint density $p\{\boldsymbol{x}, \tilde{\boldsymbol{u}}\}$, is non-trivial due to the nonlinear nature of $\boldsymbol{f}$.

Many real world problems can be described by the generic equations in (1) and (2). To demonstrate the ideas outlined later in the paper, we will use a GPS aided Inertial Navigation System (INS) as an application. State space approaches to Inertial Navigation Systems (INS) have a state evolution equation similar to (1) and almost all practical real time implementations of aided INS use an EKF to estimate the error state assuming a linearized error state propagation and measurement model. Hence accurate linearization is essential to ensuring the success of such integrations.

The following subsection briefly reviews the Extended Kalman Filter (EKF) with is based on this idea. Section I-B reviews some popular nonlinear estimation methods.

A. Linearization based methods

Linearization based estimation methods like the EKF seek to estimate the error accrued in integration of $\dot{\hat{\boldsymbol{x}}} = \boldsymbol{f}(\hat{\boldsymbol{x}}, \hat{\boldsymbol{u}})$. The error in the estimate $\hat{\boldsymbol{x}}(t)$ is defined as $\delta\boldsymbol{x}(t) = \boldsymbol{x}(t) - \hat{\boldsymbol{x}}(t)$, and it evolves in time according to

$$\delta\dot{\boldsymbol{x}}(t) = \boldsymbol{f}(\boldsymbol{x}(t), \boldsymbol{u}(t)) - \boldsymbol{f}(\hat{\boldsymbol{x}}(t), \hat{\boldsymbol{u}}(t)). \tag{4}$$

Linearization based algorithms approximate (4) by truncating the Taylor series expansion of $\boldsymbol{f}$ around $(\hat{\boldsymbol{x}}, \hat{\boldsymbol{u}})$ to first order to derive an approximate error state evolution model as

$$\delta\dot{\boldsymbol{x}}(t) = \boldsymbol{A}(t)\delta\boldsymbol{x}(t) + \boldsymbol{G}(t)\delta\boldsymbol{u}(t) \tag{5}$$

where $\boldsymbol{A}(t), \boldsymbol{G}(t)$ are time-varying matrices obtained by computing the Jacobian of $\boldsymbol{f}$ with respect to $\boldsymbol{x}$ and $\boldsymbol{u}$ respectively.

An EKF estimator is optimal [12] in the sense of minimizing the Mean Square Error (MSE), if linearization is valid and sensor measurement noise in $\tilde{\boldsymbol{u}}$ and $\tilde{\boldsymbol{y}}$ are white and Gaussian. Though the EKF algorithm is fast and a computationally inexpensive approach (esp. when using scalar sequential updates), if linearization errors in (5) are not negligible then the behavior of an EKF is unpredictable and linear propagation of error state covariance according to (5) does not necessarily reflect the actual error in the state.

B. Nonlinear Sampling based methods

Alternative estimation paradigms like the Particle filter [1] do not require the system to be linear, but large initial uncertainties can cause severe degeneracy of particles in a short time. For example if the measurement noise is assumed to be Gaussian then the weights are penalized exponentially according to their measurement residuals. A brute force method to mitigate the degeneracy issue is to use a large number of particles but the disadvantage of this approach is that

978-1-61284-799-3/11/$26.00 ©2011 IEEE

it causes a huge computational burden. Estimation methods like the Unscented Kalman Filter [7] seek to mitigate this issue of computational burden by deterministically choosing candidates or sigma points and propagating them through the nonlinear function $\boldsymbol{f}$. By carefully choosing sigma points, this algorithm is in effect generalizing the EKF by approximating the nonlinear function $\boldsymbol{f}$ up to higher orders of estimation error [20]. Here again, large uncertainties in state initializations would require an increased number of sigma points to be able to model the higher order moments of the *a-posteriori* probability density of state.

In this paper we propose a real time method to identify error states in a nonlinear system that cause significant deviation from the linearized error state model. After identifying those states, we propose a near-real time approach to estimate such states such that the linearization approach is valid again. Once we determine the validity of the linearization assumption, we integrate the states using the faster EKF approach. We demonstrate the idea in theory and simulation on a $2D$ GPS aided INS (e.g. a robot equipped with an IMU navigating a flat plane).

The outline of this paper is as follows: Section II-A discusses the generalized Bayes' solution and Section II-B discusses the linearized *Maximum-A-Posteriori* (MAP) solution to (3). Section III describes the proposed near-real time based initialization approach. Section IV-A introduces notation that is specific to the $2D$ GPS-INS application. Section IV-C describes kinematics and measurement error modeling of a $2D$ GPS-INS. Section IV-F reviews some state initialization approaches in GPS-INS. Section V provides some simulation results for the proposed idea and Section VI concludes the paper.

II. Bayesian solutions

Let the measurement of system inputs $\boldsymbol{u}$ be modeled as [6]

$$\tilde{\boldsymbol{u}} = \boldsymbol{u} + \boldsymbol{b} + \boldsymbol{\omega} \tag{6}$$

where $\boldsymbol{b}$ and $\boldsymbol{\omega}$ denote additive bias and sensor noise respectively. Sensor biases are nuisance parameters that should be estimated for improved system performance. Augmenting system state with the bias states $\boldsymbol{b}$, we define the augmented state as $\bar{\mathbf{x}}^\top = \begin{bmatrix} \boldsymbol{x}^\top & \boldsymbol{b}^\top \end{bmatrix}$.

A. Generalized Bayesian solution

We can rewrite (3) in terms of the augmented state vector $\bar{\mathbf{x}} \in \mathbb{R}^{N+M}$ as

$$\hat{\bar{\mathbf{x}}} = \arg\max_{\bar{\mathbf{x}}} \left(p\{\bar{\mathbf{x}} | \tilde{\boldsymbol{y}}, \tilde{\boldsymbol{u}}\} \right) = \arg\max_{\bar{\mathbf{x}}} \left(p\{\tilde{\boldsymbol{y}} | \bar{\mathbf{x}}, \tilde{\boldsymbol{u}}\} p\{\bar{\mathbf{x}}, \tilde{\boldsymbol{u}}\} \right). \tag{7}$$

In order to solve (7) we need to compute $p\left\{\tilde{\boldsymbol{y}} | \bar{\mathbf{x}}, \tilde{\boldsymbol{u}}\right\}$ and $\boldsymbol{p}\left\{\bar{\mathbf{x}}, \tilde{\boldsymbol{u}}\right\}$. Since $\boldsymbol{n}$ appears additively in (2), it is straightforward to compute

$$p\{\tilde{\boldsymbol{y}} | \bar{\mathbf{x}}, \tilde{\boldsymbol{u}}\} = p\{\tilde{\boldsymbol{y}} | \bar{\mathbf{x}}\} = p_{\boldsymbol{n}}\left\{\tilde{\boldsymbol{y}} - \boldsymbol{h}(\boldsymbol{x})\right\} \tag{8}$$

where p_n denotes the probability density of additive measurement noise. The joint density function of the state $p\{\bar{\mathbf{x}}, \tilde{\boldsymbol{u}}\}$ can be derived as $p\{\bar{\mathbf{x}}, \tilde{\boldsymbol{u}}\} = p\{\bar{\mathbf{x}} | \tilde{\boldsymbol{u}}, \bar{\mathbf{x}}_0\} p\{\tilde{\boldsymbol{u}} | \bar{\mathbf{x}}_0\} p\{\bar{\mathbf{x}}_0\}$ where $p\{\bar{\mathbf{x}}_0\}$ is the *a-priori* density of the state. Assuming that the biases $\boldsymbol{b}$ evolve as a random walk process according to $\dot{\boldsymbol{b}} = \boldsymbol{\omega}_b$, in concept, the density $p\{\bar{\mathbf{x}} | \tilde{\boldsymbol{u}}, \bar{\mathbf{x}}_0\}$ could be derived as

$$\frac{\partial^2}{\partial \boldsymbol{\kappa}_1 \partial \boldsymbol{\kappa}_2} P\left\{ \int_0^t \boldsymbol{f}(\boldsymbol{x}, \hat{\boldsymbol{u}}) d\tau \leq \boldsymbol{\kappa}_1 - \boldsymbol{x}(0), \boldsymbol{b}(t) \leq \boldsymbol{\kappa}_2 \right\}$$

where $\boldsymbol{b}(t) = \boldsymbol{b}(0) + \int_0^t \boldsymbol{\omega}_b$ and $\hat{\boldsymbol{u}} = \tilde{\boldsymbol{u}} - \hat{\boldsymbol{b}}$. Unless $\boldsymbol{f}$ is a simple function, deriving this joint probability is not trivial. Further $p(\tilde{\boldsymbol{u}} | \bar{\mathbf{x}}_0)$ is non-stationary as it depends on system inputs $\boldsymbol{u}$. The following subsection discusses the linearization based approximations to simplify the computation of (7).

B. Standard linearized MAP estimation

Using the initial estimate of $\boldsymbol{x}_0$, denoted by $\hat{\boldsymbol{x}}_0$ and an estimate of the system inputs $\hat{\boldsymbol{u}}$, an estimate of $\boldsymbol{x}$ is computed as

$$\hat{\boldsymbol{x}} = \hat{\boldsymbol{x}}_0 + \int_0^t \boldsymbol{f}\left(\hat{\boldsymbol{x}}, \hat{\boldsymbol{u}}\right) d\tau. \tag{9}$$

The error in the estimate defined in (9) is

$$\delta \boldsymbol{x} = \delta \boldsymbol{x}_0 + \int_0^t \boldsymbol{f}(\boldsymbol{x}, \boldsymbol{u}) - \boldsymbol{f}(\hat{\boldsymbol{x}}, \hat{\boldsymbol{u}}) d\tau. \tag{10}$$

Since $\boldsymbol{f}$ is a vector of real analytic functions, we can express it as a Taylor series in the neighborhood of $(\hat{\boldsymbol{x}}, \hat{\boldsymbol{u}})$ as

$$\boldsymbol{f}(\boldsymbol{x}, \boldsymbol{u}) = \boldsymbol{f}(\hat{\boldsymbol{x}}, \hat{\boldsymbol{u}}) + \boldsymbol{A} \delta \boldsymbol{x} + \boldsymbol{G}\left(\delta \boldsymbol{b} + \boldsymbol{\omega}\right) + \boldsymbol{T}_x \tag{11}$$

where $\boldsymbol{G} = \frac{\partial \boldsymbol{f}}{\partial \boldsymbol{u}}$, $\boldsymbol{A} = \frac{\partial \boldsymbol{f}}{\partial \boldsymbol{x}}$ evaluated at $(\hat{\boldsymbol{x}}, \hat{\boldsymbol{u}})$ and $\boldsymbol{T}_x \in \mathbb{R}^N$ denotes the higher order terms of the expansion. Substituting (11) into (10) yields

$$\delta \boldsymbol{x} = \delta \boldsymbol{x}_0 + \int_0^t \boldsymbol{A} \delta \boldsymbol{x} + \boldsymbol{G}\left(\delta \boldsymbol{b} + \boldsymbol{\omega}\right) + \boldsymbol{T}_x \, d\tau. \tag{12}$$

Note that (12) and $\delta \boldsymbol{b}(t) = \delta \boldsymbol{b}(0) + \int_0^t \boldsymbol{\omega}_b d\tau$ are the unique solution to the system that evolves according to

$$\delta \dot{\bar{\mathbf{x}}} = \bar{\mathbf{A}} \delta \bar{\mathbf{x}} + \bar{\mathbf{G}} \bar{\boldsymbol{\omega}} + \bar{\mathbf{T}}_x \tag{13}$$

where $\bar{\mathbf{A}}^\top = \left[\begin{array}{cc|c} \boldsymbol{A}^\top & \boldsymbol{G}^\top & \mathbf{0} \quad \mathbf{0} \end{array}\right]$, $\bar{\mathbf{G}}^\top = \left[\begin{array}{c|c} \boldsymbol{G}^\top & \boldsymbol{I} \end{array}\right]$, $\bar{\boldsymbol{\omega}}^\top = \left[\begin{array}{c|c} \boldsymbol{\omega}^\top & \boldsymbol{\omega}_b^\top \end{array}\right]$ and $\bar{\mathbf{T}}_x^\top = \left[\begin{array}{c|c} \boldsymbol{T}_x^\top & \mathbf{0} \end{array}\right] \in \mathbb{R}^{N+M}$.

The main assumption in this section is that the error in $(\hat{\boldsymbol{x}}, \hat{\boldsymbol{u}})$ is sufficiently small so that $\boldsymbol{T}_x$ can be ignored. Under this assumption, (12) reduces to

$$\delta \boldsymbol{x} = \delta \boldsymbol{x}_0 + \int_0^t \boldsymbol{A} \delta \boldsymbol{x} + \boldsymbol{G}\left(\delta \boldsymbol{b} + \boldsymbol{\omega}\right) \, d\tau. \tag{14}$$

Similarly the error in measurement can be expressed as

$$\delta \boldsymbol{y} = \tilde{\boldsymbol{y}} - \hat{\boldsymbol{y}} = \bar{\mathbf{H}} \delta \bar{\mathbf{x}} + \boldsymbol{n} + \boldsymbol{T}_y \tag{15}$$

where $\bar{\mathbf{H}} = \begin{bmatrix} \frac{\partial \boldsymbol{h}}{\partial \boldsymbol{x}} & \mathbf{0} \end{bmatrix}$ and $\boldsymbol{T}_y \in \mathbb{R}^P$ denotes linearization errors, which are ignored as before.

Since $\hat{\bar{\mathbf{x}}}$ is known we conclude

$$p\{\bar{\mathbf{x}}|\tilde{\boldsymbol{y}}, \tilde{\boldsymbol{u}}\} = p_{\boldsymbol{n}}\{\delta\boldsymbol{y}|\delta\bar{\mathbf{x}}, \boldsymbol{\omega}\}p(\delta\bar{\mathbf{x}}, \boldsymbol{\omega}) = p_{\boldsymbol{n}}\{\delta\boldsymbol{y}|\delta\bar{\mathbf{x}}\}p\{\delta\bar{\mathbf{x}}\}p\{\boldsymbol{\omega}\}. \tag{16}$$

From (16) we conclude that, up to linearization errors,

$$\max_{\bar{\mathbf{x}}\in\mathbb{R}^{N+M}} p(\bar{\mathbf{x}}|\tilde{\boldsymbol{y}}, \tilde{\boldsymbol{u}}) = \max_{\delta\bar{\mathbf{x}}\in\mathbb{R}^{N+M}} p_{\boldsymbol{n}}(\delta\boldsymbol{y}|\delta\bar{\mathbf{x}})p(\delta\bar{\mathbf{x}}). \tag{17}$$

Denoting $\delta\hat{\bar{\mathbf{x}}}$ as

$$\delta\hat{\bar{\mathbf{x}}} = \arg\max_{\delta\bar{\mathbf{x}}\in\mathbb{R}^{N+M}} p_{\boldsymbol{n}}(\delta\boldsymbol{y}|\delta\bar{\mathbf{x}})p(\delta\bar{\mathbf{x}}) \tag{18}$$

the result in (17) can be formally stated as the following proposition.

Proposition 2.1: When linearization errors are small, the estimate $\delta\hat{\bar{\mathbf{x}}}$ satisfies (18) if and only if $\hat{\bar{\mathbf{x}}}$ satisfies (7).

Proof: ($\Rightarrow$)Given that $\hat{\bar{\mathbf{x}}} = \bar{\mathbf{x}} + \delta\hat{\bar{\mathbf{x}}}$ and $\hat{\bar{\mathbf{x}}}$ satisfies (7), then $p(\hat{\bar{\mathbf{x}}}|\tilde{\boldsymbol{y}}, \tilde{\boldsymbol{u}}) \geq p(\bar{\mathbf{x}}^*|\tilde{\boldsymbol{y}}, \tilde{\boldsymbol{u}})$ for all other estimators $\bar{\mathbf{x}}^*$, then from (16) we conclude $p_{\boldsymbol{n}}(\delta\boldsymbol{y}|\delta\hat{\bar{\mathbf{x}}})p(\delta\hat{\bar{\mathbf{x}}}) \geq p_{\boldsymbol{n}}(\delta\boldsymbol{y}|\delta\bar{\mathbf{x}}^*)p(\delta\bar{\mathbf{x}}^*)$. Hence $\delta\hat{\bar{\mathbf{x}}}$ satisfies (18). The converse can be proved likewise. ∎

The subsequent section describes the proposed near-real time initialization approach of systems modeled as (1) and (2).

III. Near Real Time Initialization

A. Analysis

For the analysis presented here, we will consider only the contribution of the second order term in $\bar{\mathbf{T}}_x$ and $\boldsymbol{T}_y$. Let $f_j : \mathbb{R}^N \to \mathbb{R}$ and $h_i : \mathbb{R}^N \to \mathbb{R}$, denote the i^{th} and j^{th} component of $\boldsymbol{f}$ and $\boldsymbol{h}$ respectively for $0 \leq i \leq N$, $0 \leq j \leq P$. Denote the i^{th} $\left(j^{th}\right)$ element of $\bar{\mathbf{T}}_x$ $\left(\boldsymbol{T}_y\right)$ as T_x^i $\left(T_y^j\right)$ respectively. We derive

$$T_x^i = \tfrac{1}{2}\delta\bar{\mathbf{x}}^\top \boldsymbol{J}_x^i \delta\bar{\mathbf{x}} \qquad T_y^j = \tfrac{1}{2}\delta\bar{\mathbf{x}}^\top \boldsymbol{J}_y^j \delta\bar{\mathbf{x}}$$

where $\boldsymbol{J}_x^i$ $\left(\boldsymbol{J}_y^j\right)$ are the Hessian matrices of f_i (h_j) computed with respect to $\bar{\mathbf{x}}$.

The linearized model will be considered accurate if $T_x^i(T_y^i)$ are in the order of $\bar{\mathbf{G}}\bar{\boldsymbol{\omega}}(\boldsymbol{n})$, in a statistical sense. This idea is developed below. For each $0 \leq i \leq N$,

$$\begin{aligned} E\{\delta\bar{\mathbf{x}}^\top \boldsymbol{J}_x^i \delta\bar{\mathbf{x}}\} &= E\{\text{trace}\left(\delta\bar{\mathbf{x}}^\top \boldsymbol{J}_x^i \delta\bar{\mathbf{x}}\right)\} \\ &= E\{\text{trace}\left(\boldsymbol{J}_x^i \delta\bar{\mathbf{x}}\delta\bar{\mathbf{x}}^\top\right)\} \\ &= \text{trace}\left(\boldsymbol{J}_x^i \boldsymbol{P}\right) \end{aligned} \tag{19}$$

where $\boldsymbol{P}$ denotes the covariance matrix of error in $\hat{\bar{\mathbf{x}}}$. Similarly $E\{\delta\bar{\mathbf{x}}^\top \boldsymbol{J}_y^i \delta\bar{\mathbf{x}}\} = \text{trace}\left(\boldsymbol{J}_y^i \boldsymbol{P}\right)$ for each $0 \leq j \leq P$. If Q_i and R_j denote the second order moments of i^{th} and j^{th} component of $\bar{\mathbf{G}}\bar{\boldsymbol{\omega}}$ and $\boldsymbol{n}$, we conclude that the linearized model is valid if

$$\text{trace}\left(\boldsymbol{J}_x^i \boldsymbol{P}\right) < \gamma_i Q_i \qquad \text{trace}\left(\boldsymbol{J}_y^j \boldsymbol{P}\right) < \mu_j R_j \tag{20}$$

for each $0 \leq i \leq N$ and $0 \leq j \leq P$, where γ_i and μ_j are designer specific parameters. The criteria in (20) allows us to identify those states where the estimation error as characterized by $\boldsymbol{P}$ is large enough relative to the curvature (i.e. $\boldsymbol{J}_x^i$ or $\boldsymbol{J}_y^j$) such that its effect is larger than noise. This is demonstrated in Section V-A for the specific case of a $2D$ GPS-INS. One method to detect a discrepancy in the linearized model is to compare the probabilities of magnitudes of the observed measurement residuals computed from the linearized model to a designer specified threshold (λ^2). This threshold could be chosen using probabilistic principles such that it satisfies a specified performance criteria. If we observe measurement residuals whose probability of occurrence is very small according to our linearized model then that might indicate an error in the linearized model. Section III-B builds more on this idea.

B. Validation of measurements

The linearized model for the measurement residual $\delta\tilde{\boldsymbol{y}} \in \mathbb{R}^P$ is derived by ignoring $\boldsymbol{T}_y$ in (15) as

$$\delta\boldsymbol{y} = \bar{\mathbf{H}}\delta\bar{\mathbf{x}} + \boldsymbol{n}. \tag{21}$$

If the linearized model is valid (i.e. $\exists\boldsymbol{\Phi} : \mathbb{R}^{N+M} \to \mathbb{R}^{N+M}$ such that $\delta\bar{\mathbf{x}}(t) = \boldsymbol{\Phi}(t,0)\delta\bar{\mathbf{x}}(0) + \int \boldsymbol{\Phi}\bar{\mathbf{G}}\bar{\boldsymbol{\omega}}d\tau$) and uncertainty in initial state estimate $\hat{\bar{\mathbf{x}}}(0)$ is normally distributed as $\hat{\bar{\mathbf{x}}}(0) \sim \mathcal{N}(\bar{\mathbf{x}}(0), \boldsymbol{P}(0))$ then $\delta\bar{\mathbf{x}}(t) \sim \mathcal{N}(\mathbf{0}, \boldsymbol{P})$, where $\boldsymbol{P} = \boldsymbol{\Phi}\boldsymbol{P}(0)\boldsymbol{\Phi}^\top + \int \boldsymbol{\Phi}\bar{\mathbf{G}}\boldsymbol{Q}\bar{\mathbf{G}}^\top\boldsymbol{\Phi}^\top d\tau$. Further, if the additive measurement noise $\boldsymbol{n}$ is white and Gaussian with $\boldsymbol{n} \sim \mathcal{N}(\mathbf{0}, \boldsymbol{R})$, the residual in (21) is Gaussian whose covariance is derived as

$$\boldsymbol{S} = \bar{\mathbf{H}}\boldsymbol{P}\bar{\mathbf{H}}^\top + \boldsymbol{R}. \tag{22}$$

Using the procedure outlined in Section 4.9.1 in [3], we define a new variable $\boldsymbol{v} = \boldsymbol{\Sigma}^{-1}\boldsymbol{U}^\top\boldsymbol{\delta y}$, where $\boldsymbol{\Sigma}, \boldsymbol{U}$ are derived by resolving the positive symmetric matrix $\boldsymbol{S}$ using $LDL^\top$ decomposition as $\boldsymbol{S} = \boldsymbol{U}\boldsymbol{\Sigma}^2\boldsymbol{U}^\top$.

For a given threshold $\lambda \in \mathbb{R}^+$, we propose the following indicator function $\mathcal{I}$:

$$\mathcal{I} = \begin{cases} 1 & \boldsymbol{v}^\top\boldsymbol{v} \leq \lambda^2 \\ 0 & \boldsymbol{v}^\top\boldsymbol{v} > \lambda^2. \end{cases} \tag{23}$$

Using the fact $\boldsymbol{\delta y} \sim \mathcal{N}(\mathbf{0}, \boldsymbol{S})$, we can derive the stochastic properties of $\boldsymbol{v}^\top\boldsymbol{v}$. If linearization errors are indeed small then, $\boldsymbol{v}^\top\boldsymbol{v}$ is Chi-square distribution with P degrees of freedom. The probability density function of $\boldsymbol{v}^\top\boldsymbol{v}$ is given by $f_{\boldsymbol{v}^\top\boldsymbol{v}}(s) = \frac{1}{2^{\frac{P}{2}}\Gamma(\frac{P}{2})}s^{\frac{P}{2}-1}\exp\{-\frac{s}{2}\}$ for $s \geq 0$. Given $q \in (0,1)$, the corresponding threshold λ can be computed from the P^{th} order Chi-square cumulative distribution function such that $\text{Prob}\{\boldsymbol{v}^\top\boldsymbol{v} \leq \lambda^2\} = q$.

C. Near Real Time Estimation

Without loss of generality, let the state vector be organized as $\bar{\mathbf{x}}^\top = \begin{bmatrix} \boldsymbol{\zeta}_l^\top & | & \boldsymbol{\zeta}_{nl}^\top \end{bmatrix}$. The symbol $\boldsymbol{\zeta}_{nl} \in \mathbb{R}^L$ represents the states with error large enough that, when they are observable, cause $\mathcal{I} = 0$ in (23) to trigger. While $\boldsymbol{\zeta}_l \in \mathbb{R}^{M+N-L}$ represent the remaining states, for which (23) indicates that linearization is valid.

The central contribution of the paper is a method by which, over intervals of time where portions of $\boldsymbol{\zeta}_{nl}$ become

observable, errors in $\boldsymbol{\zeta}_{nl}$ within the observable subspace can be decreased to the level where the standard EKF method becomes practical. During such time intervals, due to the magnitude of $\boldsymbol{\zeta}_{nl}$ linearization based techniques are not reliable.

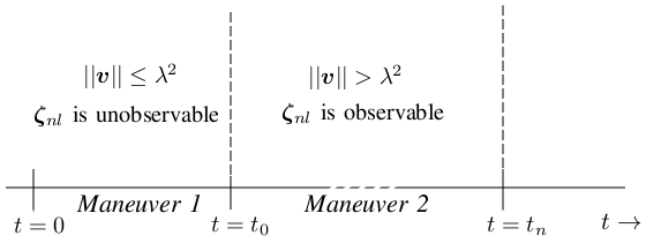

Fig. 1. In $[0, t_0]$ the observable states are sufficiently accurate such that $\boldsymbol{v}^\top \boldsymbol{v} < \lambda^2$. The system enters *Maneuver 2* at time $t = t_0$ and components of errors in $\boldsymbol{\zeta}_{nl}$ become observable. The time t_n is such that $\boldsymbol{\zeta}_{nl}(t_0)$ is observable from measurements $(\tilde{\boldsymbol{u}}(\tau), \tilde{\boldsymbol{y}}(\tau))$, $t_0 < \tau < t_n$.

In this paper, an alternative Near Real Time (NRT) Bayesian method is proposed, which is described below. Consider the situation depicted in Figure 1. In time $[0, t_0]$, the system is undertaking a trajectory called *Maneuver 1*. Assume that during this time a significant portion of the error in $\boldsymbol{\zeta}_{nl}$ lies in the unobservable subspace and hence cannot be detected by measurements $\tilde{\boldsymbol{y}}$. During *Maneuver 1* the observable states are sufficiently accurate to allow the EKF approach to succeed. An example of this is a typical stationary GPS aided INS initialization where $\boldsymbol{\zeta}_{nl}$ spans portions of the attitude and IMU biases. At time $t = t_0$, the system enters *Maneuver 2* when previously unobservable states become observable with errors too large to allow accurate linearization. Since $\boldsymbol{\zeta}_{nl}(t_0)$ is observable using measurements in $\tilde{\boldsymbol{y}}(t)$, $t_0 < t < t_n$, it is possible to initialize $\boldsymbol{\zeta}_{nl}(t_0)$ such that $\boldsymbol{v}^\top \boldsymbol{v} \leq \lambda^2$ for all $t_0 < \tau < t_n$. This idea is outlined as Algorithm 1.

Algorithm 1 Near-real time initialization

// $0 \leq \tau \leq t_0$
while $\boldsymbol{v}^\top \boldsymbol{v} < \lambda^2$ **do**
  EKF: $\hat{\boldsymbol{x}}(\tau) = \int \boldsymbol{f}(\hat{\boldsymbol{x}}, \hat{\boldsymbol{u}})$, $\hat{\boldsymbol{b}}(\tau) = \hat{\boldsymbol{b}}(0)$, $\delta\hat{\bar{\mathbf{x}}}(\tau) = E\{\delta\bar{\mathbf{x}}(\tau)|\delta\boldsymbol{y}(\tau)\}$
  $\boldsymbol{v}(\tau) \leftarrow \boldsymbol{\Sigma}^{-1}\boldsymbol{U}^\top \delta\boldsymbol{y}(\tau)$
end while
// $t_0 \leq \tau \leq t_n$
if $\mathcal{O}(\tilde{\boldsymbol{u}}(\tau), \tilde{\boldsymbol{y}}(\tau))$ **then**
  Initialize: $\boldsymbol{\zeta}_{nl}(t_0) \leftarrow \mathcal{I}(\tilde{\boldsymbol{u}}(\tau), \tilde{\boldsymbol{y}}(\tau))$ using a MAP estimator.
end if
Re-integrate via EKF: $\hat{\boldsymbol{x}}(\tau) = \int \boldsymbol{f}(\hat{\boldsymbol{x}}, \hat{\boldsymbol{u}})$, $\hat{\boldsymbol{b}}(\tau) = \hat{\boldsymbol{b}}(t_0)$, $\delta\hat{\bar{\mathbf{x}}}(\tau) = E\{\delta\bar{\mathbf{x}}|\delta\boldsymbol{y}\}$

In Algorithm 1, the indicator function $\mathcal{O} : \mathbb{R}^{M+P} \times [t_0, t_n] \rightarrow \{0, 1\}$ returns 1 if $\bar{\mathbf{x}}(t_0)$ is observable from measurements $(\tilde{\boldsymbol{u}}(\tau), \tilde{\boldsymbol{y}}(\tau))$, $t_0 < \tau < t_n$ and returns 0 otherwise. This observability test is based on the well understood observability conditions for linear systems. This condition is critical, for otherwise trying to initialize an unobservable state from noisy measurements can lead to erroneous results. The function $\mathcal{I} : \mathbb{R}^{M+P} \times [t_0, t_n] \rightarrow \mathbb{R}^L$ initializes $\boldsymbol{\zeta}_{nl}(t_0)$ based on observables $(\tilde{\boldsymbol{u}}(\tau), \tilde{\boldsymbol{y}}(\tau))$. A method to achieve this is through nonlinear least squares minimization, provided a unique global minima exists for the given cost function (existence is guaranteed if the cost function is continuous and the domain is compact, uniqueness requires proof) and achievable in a finite number of iterations. There are methods that achieve off-line over long time intervals (e.g. Bundle adjustment [19], Square root SAM [2]), but we are proposing doing the nonlinear optimization on-line over short intervals, to drive observable states to the point where second order errors are small. A possible initialization function is described for the specific case of a $2D$ GPS-INS discussed in Section IV.

IV. A 2D GPS AIDED INS

A. Notation

Let the symbols b and n in the superscript denote the body and navigation frames respectively; when they are used as subscript they depict the origins of the respective frames. The symbol ${}^x\boldsymbol{p}_{yz}$ is used to express the vector from points y to z in the x frame. If ${}^a\boldsymbol{v}$ denotes a free vector $\boldsymbol{v}$ in the a frame, then the rotation matrix ${}^b_a\boldsymbol{R}$ is used to represent it in b frame as ${}^b\boldsymbol{v} = {}^b_a\boldsymbol{R}\,{}^a\boldsymbol{v}$. The symbol ${}^c\dot{\boldsymbol{x}}$ denotes the time derivative of ${}^c\boldsymbol{x}$ vector in the c frame.

The subsequent subsections briefly discuss the kinematics of a $2D$ INS and GPS measurement models.

B. Introduction

Consider a rover in a $2D$ world whose navigation state can be fully described by

$$\boldsymbol{x}^\top = \begin{bmatrix} {}^n\boldsymbol{p}_{nb}^\top & {}^n\boldsymbol{v}_{nb}^\top & \psi \end{bmatrix}$$

where ${}^n\boldsymbol{p}_{nb}{}^\top \in \mathbb{R}^2$, ${}^n\boldsymbol{v}_{nb}{}^\top \in \mathbb{R}^2$, $\psi \in [-\pi, \pi]$ denote the position, velocity and attitude of the rover in the $2D$ world. We assume that the rover moves in the forward direction (defined relative to the body frame) without slipping in other directions. The rover is equipped with a $1D$ accelerometer and a yaw rate gyroscope that measures forward acceleration and yaw rate respectively. The inertial measurements are modeled as

$$\begin{aligned} {}^b\tilde{a}_f &= {}^b a_f + b_a + n_a \\ {}^b\tilde{\omega}_y &= {}^b\omega_y + b_\omega + n_\omega \end{aligned}$$

where ${}^b a_f$ denotes the forward acceleration and ${}^b\omega_y$ denote the yaw rate about the body frame, b_a, b_ω and n_a, n_ω represent the biases and additive noise in those sensors respectively.

C. 2D INS Kinematics & GPS Measurement model

The kinematic equations are

$$\begin{aligned} {}^n\dot{\boldsymbol{p}}_{nb} &= {}^n\boldsymbol{v}_{nb} && (24) \\ {}^n\dot{\boldsymbol{v}}_{nb} &= {}^b\omega_y \boldsymbol{\Lambda}_1^\top {}^b\boldsymbol{v}_{nb} + {}^n_b\boldsymbol{R}\,{}^b\boldsymbol{a}_{nb} && (25) \\ \dot{\psi} &= {}^b\omega_y && (26) \end{aligned}$$

where ${}^b\boldsymbol{a}_{nb}^\top = \begin{bmatrix} {}^b a_f & 0 \end{bmatrix}$ and

$${}^n_b\boldsymbol{R} = \begin{bmatrix} \cos\psi & -\sin\psi \\ \sin\psi & \cos\psi \end{bmatrix},\ \boldsymbol{\Lambda}_1 = \begin{bmatrix} -\sin\psi & \cos\psi \\ -\cos\psi & -\sin\psi \end{bmatrix}.$$

The augmented navigation state $\bar{\mathbf{x}} \in \mathbb{R}^7$ is derived as

$$\bar{\mathbf{x}}^\top = \begin{bmatrix} \boldsymbol{x}^\top & b_\omega & b_a \end{bmatrix}.$$

Equations $(24-26)$ correspond to $\boldsymbol{f}$ in the generic nonlinear model described in (1).

As stated earlier, it is difficult to compute the stochastic properties of $\bar{\boldsymbol{x}}$ due to the nonlinear nature of $(24-26)$. The EKF propagates the error covariance using a linearized approximation of the error state evolution. Let the augmented error state vector be defined as

$$\delta\bar{\mathbf{x}}^\top = \begin{bmatrix} {}^n\delta\boldsymbol{p}_{nb}^\top & {}^n\delta\boldsymbol{v}_{nb}^\top & \delta\psi & \delta b_\omega & \delta b_a \end{bmatrix}.$$

Assume a random walk model for the sensor biases

$$\dot{b}_a = n_{b_a} \quad (27)$$
$$\dot{b}_\omega = n_{b_\omega} \quad (28)$$

where n_{b_a} and n_{b_ω} are random processes. Using $(24-26)$ and $(27-28)$ the error state dynamic equations equations are derived to first order as

$${}^n\delta\dot{\boldsymbol{p}}_{nb} = {}^n\delta\boldsymbol{v}_{nb} \quad (29)$$
$${}^n\delta\dot{\boldsymbol{v}}_{nb} = {}^b\hat{\omega}_y\hat{\boldsymbol{\Lambda}}_1^\top\,{}^b_n\hat{\boldsymbol{R}}\,{}^n\delta\boldsymbol{v}_{nb} - \hat{\boldsymbol{\Lambda}}_1^{\top\,b}\hat{\boldsymbol{v}}_{nb}\left(\delta b_\omega + n_\omega\right) + \hat{\boldsymbol{\Lambda}}_2\left(\delta b_a + n_a\right) + \hat{\boldsymbol{\Lambda}}_3\delta\psi \quad (30)$$
$$\delta\dot{\psi} = -\delta b_\omega - n_\omega \quad (31)$$
$$\delta\dot{b}_\omega = n_{b_\omega} \quad (32)$$
$$\delta\dot{b}_a = n_{b_a} \quad (33)$$

where $\boldsymbol{\Lambda}_2^\top = -\begin{bmatrix} \cos\hat{\psi} & \sin\hat{\psi} \end{bmatrix}$ and

$$\boldsymbol{\Lambda}_3 = \boldsymbol{\Lambda}_1^\top\boldsymbol{\Lambda}_1\,{}^n\hat{\boldsymbol{v}}_{nb}\,{}^b\hat{\omega}_y - {}^n_b\boldsymbol{R}^b\hat{\boldsymbol{v}}_{nb}\,{}^b\hat{\omega}_y + \hat{\boldsymbol{\Lambda}}_1^{\top\,b}\hat{\boldsymbol{a}}_{nb}$$

which can be written in matrix form as

$$\delta\dot{\bar{\mathbf{x}}}(t) = \bar{\mathbf{A}}(t)\delta\bar{\mathbf{x}}(t) + \bar{\mathbf{G}}(t)\bar{\boldsymbol{\omega}}(t) \quad (34)$$

where $\bar{\boldsymbol{\omega}}^\top = \begin{bmatrix} n_\omega & n_a & n_{b_\omega} & n_{b_a} \end{bmatrix}$ such that $\bar{\boldsymbol{\omega}} \sim \mathcal{N}(\mathbf{0}, \boldsymbol{Q})$ and $\boldsymbol{Q}$ is the noise power spectral density.

D. GPS Measurement updates

Assume that there are 2 satellites in this $2D$ world at known locations ${}^n\boldsymbol{p}_j$, $j \in \{1,2\}$. The range measurement at time t corresponding to the j^{th} satellite is modeled as

$$\tilde{y}_j(t) = ||{}^n\boldsymbol{p}_{nb}(t) - {}^n\boldsymbol{p}_j|| + \omega(t)$$

where $\omega \sim \mathcal{N}(0, R)$ is additive Gaussian white noise. The j^{th} measurement residual, defined as $\delta y = y - \tilde{y}$ is modeled as a function of $\delta\bar{\mathbf{x}}$

$$\delta y_j(t) = \boldsymbol{H}_j\delta\bar{\mathbf{x}}(t) + \boldsymbol{\omega}(t) \quad (35)$$

where $\boldsymbol{H}_j = \begin{bmatrix} \frac{{}^n\boldsymbol{p}_{nb}(t) - {}^n\boldsymbol{p}_j}{||{}^n\boldsymbol{p}_{nb}(t) - {}^n\boldsymbol{p}_j||} & \mathbf{0} & 0 & 0 & 0 \end{bmatrix}$.

E. Observability conditions

Define the following rover maneuvers during the time $[0, t_n]$:

1) *Maneuver 1*: Rover is at rest for all $\tau \in [0, t_0)$.
2) *Maneuver 2*: Rover undergoes non-zero constant acceleration along a straight line for all $\tau \in [t_0, t_n]$.

The following proposition is stated but not proved:

Proposition 4.1: The rover state is not fully observable from range measurements during *Maneuver 1*. The rover state is fully observable when *Maneuver 1* is followed by *Maneuver 2* using range measurements.

Proof: Solving $(29-33)$, we derive

$$\delta\bar{\mathbf{x}} = \boldsymbol{\Phi}(t,0)\delta\bar{\mathbf{x}} \quad (36)$$

where

$$\boldsymbol{\Phi} = \begin{bmatrix} \boldsymbol{I} & \int\exp\left\{\int\boldsymbol{\Xi}\right\} & \int\boldsymbol{\Lambda}_3 & -\iint\boldsymbol{\Lambda}_1^{\top\,b}\boldsymbol{v}_{nb} & \frac{\boldsymbol{\Lambda}_2}{2}t^2 \\ \mathbf{0} & \exp\left\{\int\boldsymbol{\Xi}\right\} & \boldsymbol{\Lambda}_3 & -\int\boldsymbol{\Lambda}_1^{\top\,b}\boldsymbol{v}_{nb} & \boldsymbol{\Lambda}_2 t \\ \mathbf{0} & \mathbf{0} & \boldsymbol{I} & \boldsymbol{I}t & \mathbf{0} \\ \mathbf{0} & \mathbf{0} & \mathbf{0} & \boldsymbol{I} & \mathbf{0} \\ \mathbf{0} & \mathbf{0} & \mathbf{0} & \mathbf{0} & \boldsymbol{I} \end{bmatrix}$$
$$\boldsymbol{\Xi} = {}^b\hat{\omega}_y\hat{\boldsymbol{\Lambda}}_1^\top\,{}^b_n\hat{\boldsymbol{R}}$$

and process noise has been ignored since it is irrelevant to observability analysis. Assume that for all $t \in [0, t_n]$, the line-of-sight vectors to satellites are not collinear. Under this assumption, we can reduce the measurement equation to

$${}^n\delta\tilde{\boldsymbol{p}}_{nb} = \bar{\boldsymbol{H}}\delta\bar{\mathbf{x}} \quad (37)$$

where $\bar{\boldsymbol{H}} = \begin{bmatrix} \boldsymbol{I} & \mathbf{0} & 0 & 0 & 0 \end{bmatrix}$ and measurement noises are ignored. It can be shown that if for each $t \in [0, t_n]$,

$$\bar{\boldsymbol{H}}\boldsymbol{\Phi}(0,t)\boldsymbol{v} = \mathbf{0} \quad (38)$$

implies $\boldsymbol{v} = \mathbf{0}$, then the observability gramian has full rank. Let $\boldsymbol{v}^\top = \begin{bmatrix} \boldsymbol{v}_1^\top & \boldsymbol{v}_2^\top & \boldsymbol{v}_3^\top & \boldsymbol{v}_4^\top & \boldsymbol{v}_5^\top \end{bmatrix}$ such that it satisfies (38). For all $t \in (0, t_0)$, we derive

$$\boldsymbol{v}_1 + \boldsymbol{v}_2 t + \frac{\boldsymbol{\Lambda}_2}{2}\boldsymbol{v}_5 t^2 = \mathbf{0}. \quad (39)$$

By repeated differentiation of (39), we derive

$$\boldsymbol{v}_1 = \boldsymbol{v}_2 = \boldsymbol{v}_5 = \mathbf{0}. \quad (40)$$

Using (38) and (40), we derive for all $t \in (t_0, t_n)$ as

$$\boldsymbol{\Lambda}_1^{\top\,b}\tilde{\boldsymbol{a}}_{nb}\boldsymbol{v}_3 - \iint\boldsymbol{\Lambda}_1^{\top\,b}\boldsymbol{v}_{nb}\boldsymbol{v}_4 = \mathbf{0} \quad (41)$$

Differentiating (41) twice, we derive $\boldsymbol{v}_4 = \mathbf{0}$. Substituting $\boldsymbol{v}_4 = \mathbf{0}$ into (41), we derive $\boldsymbol{v}_5 = \mathbf{0}$. Hence $\boldsymbol{v} = \mathbf{0}$. ■

Using linearized observability analysis, we can show that for during *Maneuver 1* with at least ranging measurements from two satellites with non-collinear line-of-sight vectors, ${}^n\boldsymbol{p}_{nb}$, ${}^n\boldsymbol{v}_{nb}$ and b_a are observable. The attitude and gyroscope bias states are unobservable until the vehicle accelerates.

F. Literature review

Initial uncertainty in position and velocity affect the error state evolution linearly (see (29)) and hence it is accounted for by linear covariance propagation models. If the rover is initially known to be at rest then a reliable estimate of gyroscope biases can be obtained by averaging gyroscope measurements. Hence, yaw is the only state with a potential to have large uncertainty, because it is unobservable through standard range measurements. In this idealized $2D$ system, we are able to estimate the forward accelerometer biases also, but in real-world systems, this is not possible as errors in alignment are coupled with the accelerometer biases.

1) Sensors: It is known that in any linearization based aided INS, attitude can be a significant source of nonlinearity, hence a significant amount of research has been conducted into attitude initialization. In [15], the author uses 2 tilt sensors to measure initial roll and pitch and estimates accelerometer biases while the vehicle is stationary. Yaw and heading is initialized after the rover begins to move. The approaches in [14] and [21], use the accelerometer measurements to initialize roll and pitch and a magnetic compass to initialize yaw. In a related work [17], the author uses a sun sensor to initialize yaw. Approaches in [9], [10], [11] etc., use double differenced carrier phase measurements (after resolving integer ambiguities) from three or more GPS antennas mounted at at known relative locations to estimate $3D$ attitude.

2) Methods: In [5], the author uses a Particle Filter to solve the in flight misalignment problem where initial uncertainty is large. In [18], [16], large heading errors are accommodated by alternative modeling (i.e. estimating the sine and cosine of yaw separately by augmenting them in the state vector). The approach in [4] uses standard fixed point smoother to initialize the system in near-real time. Particle filters have also been considered as a solution to the aided INS problem. A 3 state $2D$ GPS aided odometer based navigation system requires about 2000 particles to achieve lane-level accuracy [13]. A 7 state $2D$ GPS aided INS simulation outlined in Section V required 5000 particles to provide similar navigation performance to the near-real time initialization approach. The number of particles required to approximate the *a-posteriori* density grows exponentially with the increase in state dimension. In general if m particles are used sample a single dimensional probability density and the *a-posteriori* density is d dimensional then the number of required particles is m^d.

V. Simulation Results

The purpose of the this subsection is to demonstrate the use of the methodology in Section III of this paper to identify the states whose uncertainty causes significant deviation from the ideal linearized model. In the simulation the power spectral density of the accelerometer and gyroscope measurements noise were assumed to be 10^{-3}(m/s/s)^2 Hz^{-1} and 10^{-7}(rad/s)^2 Hz^{-1}. The bias random walk parameters in $(27-28)$ were assumed to be $n_{b_\omega} \sim \mathcal{N}(0, \sigma_{b_\omega})$, $n_{b_a} \sim \mathcal{N}(0, \sigma_{b_a})$ where $\sigma^2_{b_a} = 10^{-7}$(m/s/s/s)^2 Hz^{-1}, $\sigma^2_{b_\omega} = 10^{-11}$(rad/s/s)^2 Hz^{-1} for the accelerometer and gyroscope respectively. The raw IMU measurements are shown in Figure 2. It can be shown that the full linearized error state is observable at time $t = 19$ s. The initial uncertainty was assumed to be Gaussian with $diag\,(\boldsymbol{P}(0)) = \begin{bmatrix} 0.5 & 0.5 & 0.1 & 0.1 & 0.67\pi & 10^{-3} & 5\times10^{-3} \end{bmatrix}$ with all correlations set to zero. The error in initial yaw was $120\,\mathrm{deg}$.

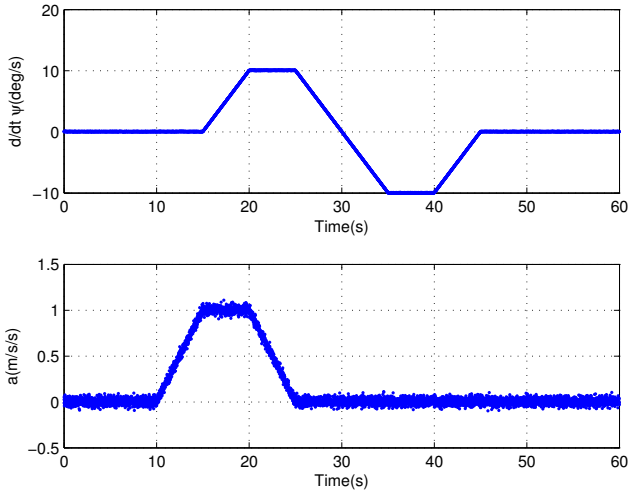

Fig. 2. The IMU measurements as the rover executed a simulated trajectory. The power spectral density of the accelerometer and gyroscope measurements noise were assumed to be 10^{-3}(m/s/s)^2 Hz^{-1} and 10^{-7}(rad/s)^2 Hz^{-1}.

A. Nonlinear effects of states

Given the kinematic system described by $(24-26)$, the exact error state dynamic is derived as (13). From $(29-33)$ we see that only (30) is an approximation (i.e. truncated at the first order of Taylor series) and the rest are exact, hence $\bar{\mathbf{T}}_x$ has the form $\bar{\mathbf{T}}_x^\top = \begin{bmatrix} \mathbf{0} & T_x^3 & T_x^4 & 0 & 0 & 0 \end{bmatrix}$. Considering the contribution of only the second order terms, we derive

$$T_x^3 = \tfrac{1}{2}\delta\bar{\mathbf{x}}\boldsymbol{J}_x^3\delta\bar{\mathbf{x}}^\top \qquad T_x^4 = \tfrac{1}{2}\delta\bar{\mathbf{x}}\boldsymbol{J}_x^4\delta\bar{\mathbf{x}}^\top \tag{42}$$

where

$$\boldsymbol{J}_x^{3\top} = \begin{bmatrix} \mathbf{0}_{7\times4} & \boldsymbol{C}_3 & \mathbf{0}_{7\times2} \end{bmatrix},$$
$$\boldsymbol{J}_x^{4\top} = \begin{bmatrix} \mathbf{0}_{7\times4} & \boldsymbol{C}_4 & \mathbf{0}_{7\times2} \end{bmatrix}$$

and

$$\boldsymbol{C}_3^\top = \begin{bmatrix} \mathbf{0} & {}^b\hat{\omega}_y & 0 & \boldsymbol{\alpha}^b\hat{\boldsymbol{v}}_{nb} & v_1 & 0 \end{bmatrix}$$
$$\boldsymbol{C}_4^\top = \begin{bmatrix} \mathbf{0} & 0 & {}^b\hat{\omega}_y & \boldsymbol{\beta}^b\hat{\boldsymbol{v}}_{nb} & v_2 & 0 \end{bmatrix}$$

where $\boldsymbol{\alpha} = \frac{1}{2}\begin{bmatrix} -\sin\psi^b\hat{\omega}_y + \cos\psi & -\cos\psi^b\hat{\omega}_y - \sin\psi \end{bmatrix}$, $\boldsymbol{\beta} = \frac{1}{2}\begin{bmatrix} \cos\psi^b\hat{\omega}_y + \sin\psi & -\sin\psi^b\hat{\omega}_y + \cos\psi \end{bmatrix}$ and ${}^n\boldsymbol{v}_{nb}^\top = \begin{bmatrix} v_1 & v_2 \end{bmatrix}$.

Similarly nonlinear effects of states on the j^{th} measurement is denoted by $T_y^j = \frac{1}{2}\delta{}^n\boldsymbol{p}_{nb}{}^\top\boldsymbol{C}_y{}^n\delta\boldsymbol{p}_{nb}$, where $\boldsymbol{C}_y = \frac{\boldsymbol{I}}{\rho} - \frac{({}^n\boldsymbol{p}_{nb} - {}^n\boldsymbol{p}_j)({}^n\boldsymbol{p}_{nb} - {}^n\boldsymbol{p}_j)^\top}{\rho^3}$ with $\rho = ||{}^n\boldsymbol{p}_{nb} - {}^n\boldsymbol{p}_j||^2$. Note that in real world scenarios $\rho \approx 20\times10^6$m, hence

effects of T_y^j are at the 10^{-2}m level even if error in position ${}^n\delta\boldsymbol{p}_{nb} \approx 100$m. Hence (20) is satisfied with $\mu = 1$ even for large errors in ${}^n\delta\boldsymbol{p}_{nb}$.

For a motion scenario defined by the raw IMU measurements in Figure 2, the absolute value of trace($\boldsymbol{J}_x^3\boldsymbol{P}$) and trace($\boldsymbol{J}_x^4\boldsymbol{P}$) (black dots) along with Q_3 and Q_4 (red dots) is depicted in Figure 3, where Q_3 (Q_4) is the third(fourth) diagonal term in

$$\boldsymbol{Q}_d = \int_0^t \boldsymbol{\Phi}\boldsymbol{G}\boldsymbol{Q}\boldsymbol{G}^\top\boldsymbol{\Phi}^\top d\tau.$$

The EKF propagation of the error covariance matrix P takes at least 30 s to decrease to the point where (20) is satisfied. This is attributed to the fact that as the rover begins to move, errors in attitude, biases become observable and are corrected by the EKF resulting in smaller values of $diag(\boldsymbol{P})$. Note that this does not imply that errors in those states are small, because the EKF uses an invalid linearized error model. Convergence of the EKF will depend on the magnitude of the initial attitude error. Figure 4 shows the corresponding measurement residuals (blue dots) along with the residual covariance (red dots). It can be seen that attitude errors cause large measurement residuals, easily detected by (23), when the rover begins to move at $t = 10$ s.

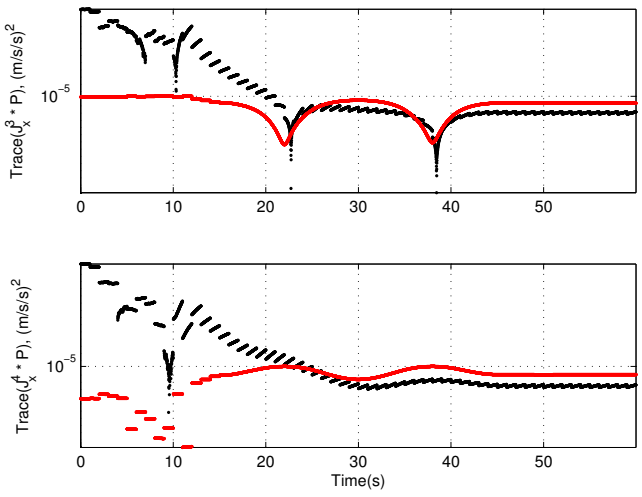

Fig. 3. The black dots denote trace($\boldsymbol{J}_x^3\boldsymbol{P}$) and trace($\boldsymbol{J}_x^4\boldsymbol{P}$) and the red dots denotes Q_3 and $Q4$.

B. Initialization of $\boldsymbol{\zeta}_{nl}$

In the previous section it was determined that for a $2D$ GPS-INS, $\boldsymbol{\zeta}_{nl} = \psi$. This section presents results of initializing $\boldsymbol{\zeta}_{nl}$ by finding the *MAP* estimate via nonlinear optimization. First we generated N_p candidates of the state $\bar{\mathbf{x}}^i$, $0 \leq i \leq N_p$ such that they differ only along the ψ direction. Assuming that $\psi \sim U[-\pi, \pi]$, the attitudes of the candidates were deterministically chosen at equal intervals in that range. The candidates

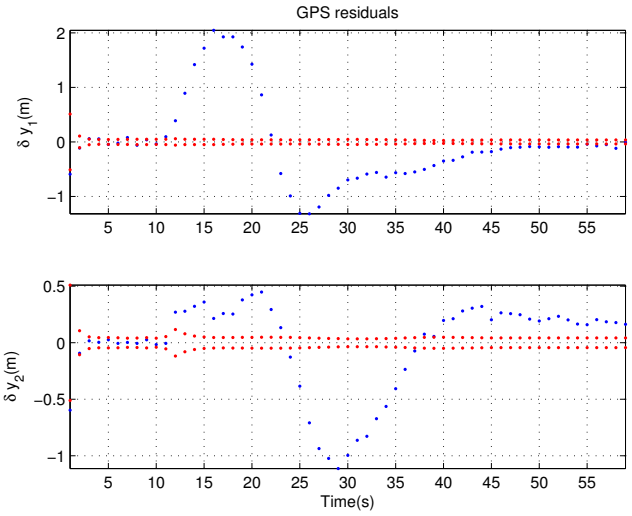

Fig. 4. GPS residuals are depicted as blue dots and the corresponding $\pm 1\sigma$ standard deviation is depicted as red dots.

were integrated through $[t_0, t_n]$ and the GPS measurements residuals generated by the i^{th} candidate was computed as $\delta\boldsymbol{Y}_i^\top = \begin{bmatrix} \delta\boldsymbol{y}_i^\top(t_1) & \dots & \delta\boldsymbol{y}_i^\top(t_j) & \dots & \delta\boldsymbol{y}_i^\top(t_n) \end{bmatrix}$ where $1 \leq j \leq n$ is the index on discrete time GPS measurements. We assign weights inversely proportional to the square-norm of the measurement residuals, i.e. the candidates are weighted according to $w_i = \left(\delta\boldsymbol{Y}_i^\top\delta\boldsymbol{Y}_i\right)^{-1}$, and the top two candidates with maximum weights are selected (say ψ_m, ψ_n). In the next iteration, N_p candidates are chosen with attitudes deterministically chosen between ψ_m and ψ_n. This iterative procedure continues till $|\psi_m - \psi_n| < \epsilon$, where ϵ is a chosen threshold (in this case $\epsilon = 3\,\text{deg}$) selected to guarantee accuracy of the linearized error model.

Figure 5 shows the normalized weights plotted against the attitudes of candidates during various iterations. In our simulations, the attitude converged in just 3 iterations when $N_p = 5$. The attitude estimate ψ_c is computed as the weighted average of the candidate attitudes in the last iteration.

Figure 6 depicts the measurement residuals (blue dots) along with its $\pm 1\sigma$ standard deviation (red dots) derived by re-integrating the state after near real time initialization. The proposed approach work even for yaw errors as high as $180\,\text{deg}$, whereas an EKF may quickly become unstable with such large attitude errors.

VI. Conclusion

Performance of linearization based algorithms using the state-space approach heavily depends on the accuracy of the linearization point. In real world applications, initialization of states is not always trivial. Errors in certain states cause a greater deviation from the linearized model than others. In this paper we propose a method to identify such states and a method to validate measurements to detect errors in the linearized model. We also proposed a near-real time approach

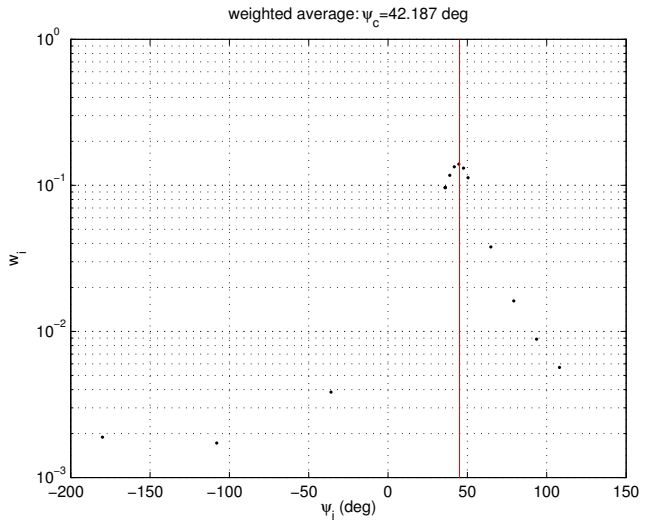

Fig. 5. The black dots depict weights of candidates whose attitudes are deterministically selected. The red line indicates the true initial attitude $(45\,\text{deg})$. In this case, the weighted average ψ_c, after coarse initialization is computed as $42.1\,\text{deg}$.

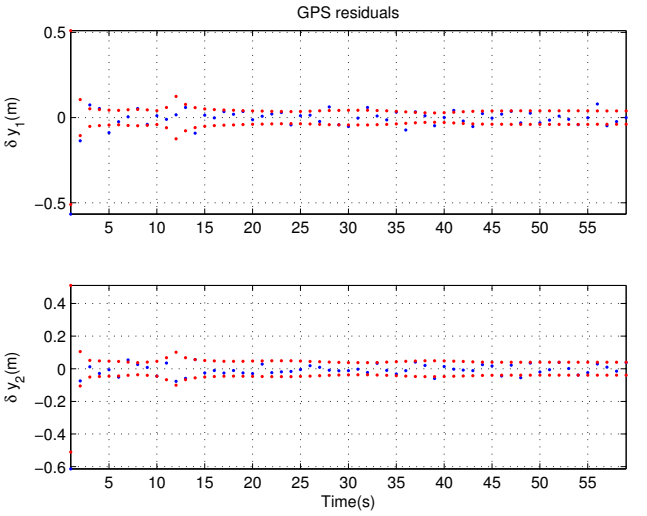

Fig. 6. GPS residuals are depicted as blue dots and the corresponding $\pm 1\sigma$ standard deviation is depicted as red dots computed by re-integrating the state after attitude initialization.

to initialization of states. The paper also demonstrates the theory on a simple 7 state $2D$ GPS aided INS.

VII. Acknowledgement

This article was prepared with support from the State of California, Business, Transportation and Housing Agency, Department of Transportation under Award 65A0261 and the DOT Federal Highway Administration Agency Award No. DTFH61-09-C-00018. The authors gratefully acknowledge this support. The contents of this paper reflect the views of the authors who are responsible for the facts and accuracy of the data presented herein. The contents do not necessarily reflect the official views or policies of the State of California or of the United States government. This report does not constitute a standard, specification, or regulation.

References

[1] M. Arulampalam, S. Maskell, N. Gordon, and T. Clapp, "A tutorial on particle filters for online nonlinear/non-Gaussian Bayesian tracking," *IEEE Trans. on Signal Processing*, vol. 50, no. 2, pp. 174–188, 2002.

[2] F. Dellaert and M. Kaess, "Square root SAM," in *Proc. of Robotics: Science and Systems*, 2005, pp. 1181–1203.

[3] J. A. Farrell, *Aided Navigation: GPS with High Rate Sensors*. McGraw Hill, 2008.

[4] M. Grewal, R. Miyasako, and J. Smith, "Application of fixed point smoothing to the calibration, alignment and navigation data of inertial navigation systems," in *Position Location and Navigation Symposium*. IEEE, 2002, pp. 476–479.

[5] Y. Hao, Z. Xiong, and Z. Hu, "Particle Filter for INS In-Motion Alignment," in *Industrial Electronics and Applications, 1ST IEEE Conference on*, 2006, pp. 1–6.

[6] C. Jekeli, *Inertial Navigation Systems with Geodetic Applications*. Walter de Gruyter, 2001.

[7] S. Julier and J. Uhlmann, "A new extension of the Kalman filter to nonlinear systems," in *Int. Symp. Aerospace/Defense Sensing, Simul. and Controls*, vol. 3, 1997, p. 26.

[8] S. M. Kay, *Fundamentals of Statistical Signal Processing, Estimation theory*. Prentice Hall PTR, 1993.

[9] G. Lachapelle, M. Cannon, G. Lu, and B. Loncarevic, "Shipborne GPS attitude determination during MMST-93," *Oceanic Engineering, IEEE Journal of*, vol. 21, no. 1, pp. 100–104, 2002.

[10] Y. Li, K. Zhang, C. Roberts, and M. Murata, "On-the-fly gps-based attitude determination using single- and double-differenced carrier phase measurements," *GPS Solutions*, vol. 8, pp. 93–102, 2004.

[11] G. Lu, M. Cannon, G. Lachapelle, and P. Kielland, "Attitude determination in a survey launch using multi-antenna GPS technologies," in *Proc. of National Technical Meeting, ION*, vol. 251, 1993, p. 260.

[12] J. S. Meditch, *Stochastic Optimal Linear Estimation and Control*. McGraw-Hill Education, August 1969.

[13] I. Miller and M. Campbell, "Particle filtering for map-aided localization in sparse GPS environments," in *Robotics and Automation. Int. Conference on*. IEEE, 2008, pp. 1834–1841.

[14] P. Miller, J. Farrell, Y. Zhao, and V. Djapic, "Autonomous underwater vehicle navigation," *Oceanic Engineering, IEEE Journal of*, vol. 35, no. 3, pp. 663–678, 2010.

[15] E. Nebot and H. Durrant-Whyte, "Initial calibration and alignment of low-cost inertial navigation units for land vehicle applications," *Journal of Robotic Systems*, vol. 16, no. 2, pp. 81–92, 1999.

[16] T. Pham, "Kalman filter mechanization for INS airstart," in *Digital Avionics Systems Conference*. IEEE, 2002, pp. 516–525.

[17] S. Roumeliotis, G. Sukhatme, and G. Bekey, "Smoother based 3d attitude estimation for mobile robot localization," in *Robotics and Automation, Int. Conf. on*, vol. 3. IEEE, 2002, pp. 1979–1986.

[18] B. Scherzinger, "Inertial navigator error models for large heading uncertainty," in *PLANS*. IEEE, 2002, pp. 477–484.

[19] B. Triggs, P. McLauchlan, R. Hartley, and A. Fitzgibbon, "Bundle adjustment: a modern synthesis," *Vision algorithms: theory and practice*, pp. 153–177, 2000.

[20] E. Wan and R. Van Der Merwe, "The unscented Kalman filter for nonlinear estimation," in *Adaptive Systems for Signal Processing, Communications, and Control Symposium. IEEE*, 2002, pp. 153–158.

[21] M. Wang, Y. Yang, R. Hatch, and Y. Zhang, "Adaptive filter for a miniature MEMS based attitude and heading reference system," in *PLANS*. IEEE, 2004, pp. 193–200.